doi.org/10.1002/hlca.202200131

RESEARCH ARTICLE

HELVETICA chimica acta

Trinodal Self-Penetrating Versus *cds* 3-Dimensional Networks Using Bis(3,2′:6′,3″-terpyridine) Building Blocks: the Solvent Makes the Difference

Simona S. Capomolla,[a] Giacomo Manfroni,[a] Alessandro Prescimone,[a] Edwin C. Constable,[a] and Catherine E. Housecroft*[a]

[a] Department of Chemistry, University of Basel, BPR 1096, Mattenstrasse 24a, CH-4058 Basel, Switzerland,
e-mail: catherine.housecroft@unibas.ch

Reactions between $Co(NCS)_2$ and $2^4,2^4$-[2,5-bis(cyclohexyloxy)-1,4-phenylene]di($1^3,2^2:2^6,3^3$-terpyridine) (**1**), $2^4,2^4$-[2,5-bis(cyclohexylmethoxy)-1,4-phenylene]di($1^3,2^2:2^6,3^3$-terpyridine) (**2**), and $2^4,2^4$-[2,5-bis(2-phenylethoxy)-1,4-phenylene]di($1^3,2^2:2^6,3^3$-terpyridine) (**3**) under conditions of crystal growth by layering at room temperature lead to 3-dimensional nets with either a *cds* or trinodal self-penetrating topology depending upon the solvents ($MeOH/C_6H_5Cl$, $MeOH/1,2\text{-}Cl_2C_6H_5$, or $MeOH/CHCl_3$) used in the crystallization experiments. The *cds* network was found for $[Co(NCS)_2(\mathbf{1})]_n{\cdot}2nC_6H_4Cl_2$, $[Co(NCS)_2(\mathbf{2})]_n{\cdot}4nC_6H_4Cl_2$, and $[Co(NCS)_2(\mathbf{3})]_n{\cdot}2.5nC_6H_5Cl$, while a trinodal self-penetrating net was observed in $[Co_2(NCS)_4(\mathbf{2})_2]_n{\cdot}5.5nCHCl_3{\cdot}0.2n$MeOH. Preliminary structural data for single crystals from the reactions of $Co(NCS)_2$ and **1** or $Co(NCS)_2$ and **3** from $MeOH/CHCl_3$ solvent combinations also evidenced the assemblies of trinodal self-penetrating nets. Both net topologies assemble from a combination of planar, 4-connecting metal and ligand nodes. The role of the solvent in directing the network type is investigated.

Keywords: cobalt, cobalt(II) thiocyanate, coordination network, lattice solvent, ligand nodes, solvent effects, 3,2′:6′,3″-terpyridine.

Introduction

The use of 3,2′:6′,3″-terpyridines (=$1^3,2^2:2^6,3^3$-terpyridines), in coordination chemistry has gained in popularity over the last decade, although this isomer of terpyridine remains less well exploited than the bis(chelating) 2,2′:6′,2″-terpyridine (=$1^2,2^2:2^6,3^2$-terpyridine) and the divergent 4,2′:6′,4″-terpyridine (=$1^4,2^2:2^6,3^4$-terpyridine; *Scheme 1*).[1–5] The coordination chemistry of derivatives of 3,2′:6′,3″-tpy was first explored by *Grafino et al.* who reported the structure of $[Zn_2(\mu\text{-}4'\text{-Ph-}3,2':6',3''\text{-tpy})(acac)_4]{\cdot}H_2O$ (4′-Ph-3,2′:6′,3″-tpy = 4′-phenyl-3,2′:6′,3″-terpyridine; Hacac = pentane-2,4-dione).[6] This revealed coordination only through the outer pyridine rings of the 3,2′:6′,3″-tpy unit. There are now around 123 structures of compounds containing metal-coordinated 3,2′:6′,3″-tpy units in the Cambridge Structural Database (CSD) version 2022.2.0,[7] (searched using ConQuest version 2022.2.0[8]), and these demonstrate that the ditopic nature of the 3,2′:6′,3″-tpy domain is the norm, with the central pyridine ring remaining non-coordinated. There are two examples in which the central pyridine ring is present as the *N*-oxide.[9] Both 3,2′:6′,3″- and 4,2′:6′,4″-tpy can be considered as having divergent donor sets. However, the conformational flexibility of the 3,2′:6′,3″-tpy unit sets it apart from the 4,2′:6′,4″-isomer which has a fixed V-shaped coordination mode (*Scheme 1*). Conformation **I** of 3,2′:6′,3″-tpy is suited to the formation of discrete dinuclear complexes, for example, with cyclic structures,[6,10–12] whereas conformations **II** and **III** are more typically encountered in coordination polymers and networks. A range of

Supporting information for this article is available on the WWW under https://doi.org/10.1002/hlca.202200131

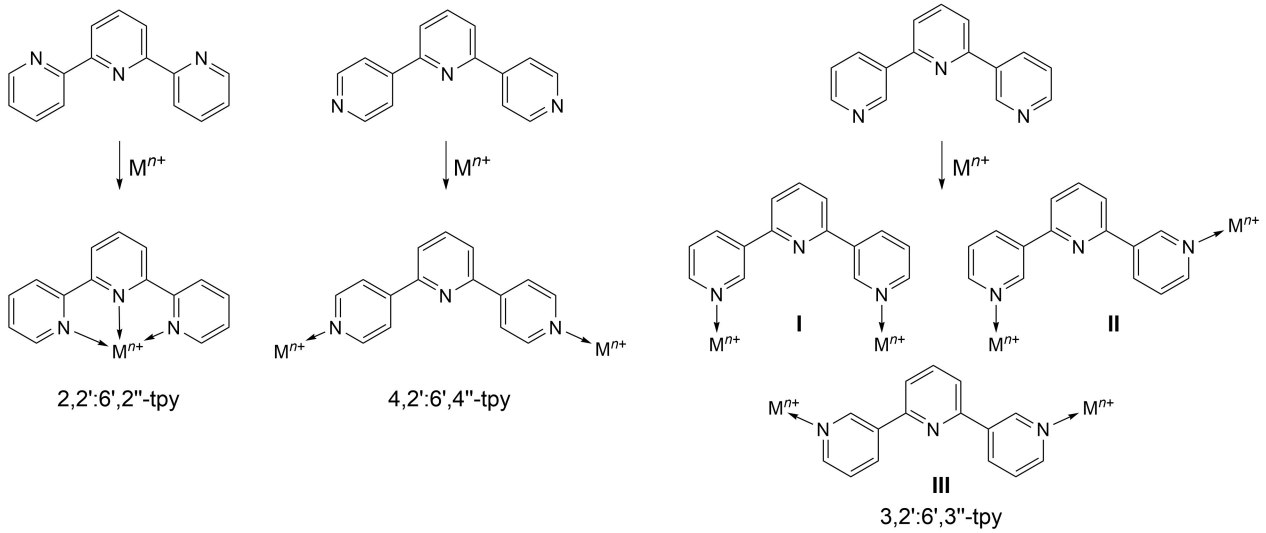

Scheme 1. Structures of three isomers of terpyridine: 2,2′:6′,2″-tpy typically behaves as a bis(chelate), 4,2′:6′,4″-tpy typically behaves as a ditopic ligand, and 3,2′:6′,3″-tpy is also a ditopic ligand but with three limiting, planar conformations **I**, **II** and **III**.

3,2′:6′,3″-terpyridines in which a functional group has been introduced into the 4′-position is known, and the conformation of the 3,2′:6′,3″-tpy domain varies with the 4′-substituent,[13–22] presumably because of packing interactions. Such conformational flexibility makes functionalized 3,2′:6′,3″-tpy ligands attractive building blocks in coordination assemblies.

Moving from a ditopic 3,2′:6′,3″-tpy unit to a tetratopic bis(3,2′:6′,3″-tpy) domain modifies the role of the ligand from a linker to a 4-connecting node, and we have recently reported a series of 3-dimensional networks directed by a combination of 4-connecting bis(3,2′:6′,3″-tpy) ligands (*Figure 1*), and a 4-connecting cobalt(II) center.[23–25] With one exception,[23] two structural motifs for $[Co(NCS)_2(L)]_n$ compounds persist: a *cds* network and a trinodal self-penetrating net.[24,25] An overview of our previous results suggested that, for the range of R groups studied, the choice of the substituent in **1** was not the deciding factor, but rather the choice of solvents for crystal growth by layering. For the general family of ligands, L, shown in *Figure 1* with R = propyl, butyl, pentyl, hexyl, heptyl or octyl, we have previously observed that a *cds* net forms when either 1,2-dichlorobenzene or chlorobenzene is used in combination with MeOH in reactions of the ligand with $Co(NCS)_2$ to give solvated $[Co(NCS)_2(L)]_n$.[25] In contrast, a trinodal, self-penetrating network formed when MeOH and chloroform were used in reactions of $Co(NCS)_2$ with L in which R = 2-ethylbutyl or 3-methylbutyl.[24] Preliminary data for crystals grown by layering an MeOH solution of $Co(NCS)_2$ over a $CHCl_3$ solution of L with R = *n*-butyl confirmed the assembly of a trinodal self-penetrating network.[25] These observations motivated us to move to more sterically demanding R groups while at the same time using different solvent mixtures for the reactions of $Co(NCS)_2$ with ligand L. A phenyl unit also has the potential for π-stacking interactions in the solid state, which may influence the assembly process. Our aim was to see if the structural trends that had so far emerged with alkyloxy substituents would be further supported when the ligand was structurally modified.

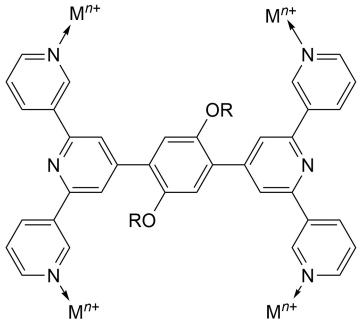

Figure 1. Structure of a general tetratopic bis(3,2′:6′,3″-tpy) ligand, L, with functionalized central arene core.

Results and Discussion

Ligand Synthesis and Characterization

The ligands selected for the investigation, **1**–**3**, are shown in *Scheme 2*. Each bears terminal cyclohexyl (Cy) or phenyl groups in the substituents attached to the central arene core of the ligand. Compound **3** was prepared as previously reported,[26] and the synthetic routes to **1** and **2** are summarized in *Scheme 2*. The second step follows the one-pot strategy described by Wang and Hanan.[27] The precursors **1a**, **1b**, **2a** and **2b** were fully characterized (see *Figures S1–S15* in the *Supporting Information*) with NMR spectra assigned using routine 2D methods (see *Experimental Section*). Attempts to record mass spectra of **1a** and **2a** (MALDI and electrospray MS) were unsuccessful. Compounds **1** and **2** were characterized by ^{1}H- and ^{13}C{^{1}H}-NMR spectroscopic methods, with signals assigned using COSY, NOESY, HMQC and HMBC techniques (see *Figures S16–S23* in the *Supporting Information*). The spectra are consistent with a single 3,2′:6′,3″-tpy environment and with the presence of the cyclohexyl units. The MALDI-TOF mass spectrum of **1** exhibited a base peak at *m/z* 736.85 arising from the $[M+H]^+$ ion (*Figure S24*), and for **2**, the base peak in the MALDI-TOF mass spectrum (*m/z* 765.04) also arose from the $[M+H]^+$ ion (*Figure S25*). The solid-state IR spectra of **1** and **2** are similar (*Figures S28* and *S29*), with strong absorptions at 2930 and 2922 cm^{-1}, respectively, assigned to the cyclohexyl groups, and absorptions in the fingerprint region arising predominantly from vibrations within the terpyridine domains. *Figure 2* displays the solution absorption spectra of **1** and **2** which are dominated by intense absorptions arising from $\pi^*\leftarrow\pi$ transitions. The spectra are reminiscent of those of structurally related 1,4-bis(*n*-alkyloxy)-2,5-bis(3,2′:6′,3″-terpyridin-4′-yl)benzene ligands.[28]

Colorless block-shaped single crystals of **1** were grown at room temperature by slow evaporation of a chloroform solution of the compound. The compound crystallizes in the monoclinic space group $P2_1/c$ with half the molecule of **1** in the asymmetric unit. The second half of the molecule is generated by inversion, and *Figure 3* shows the molecular structure. The 3,2′:6′,3″-tpy unit adopts conformation **I** (*Scheme 1*) with the angles between the least squares planes of the pyridine rings containing N1/N2 and N2/N3 being 24.9 and 19.3°. Bond lengths and angles are unexceptional, although it is worth noting that a comparison of the bond lengths of O1–C17 = 1.377(5) Å and O1–C19 = 1.457(5) Å indicates extension of π-conjugation from the arene ring across C17–O1. The C17–O1–C19 bond angle of 119.3(3)° is consistent with sp^2 hybridization. The pyridine ring containing N2 is twisted through 38.5° with respect to the plane of the arene ring containing atom C15, consistent with minimizing inter-ring H···H contacts. The $CHCl_3$ molecule is disordered and has been modelled over two sites of equal occupancies. In the lattice, adjacent molecules of **1** engage in face-to-face π-stacking interactions between thee pyridine rings containing

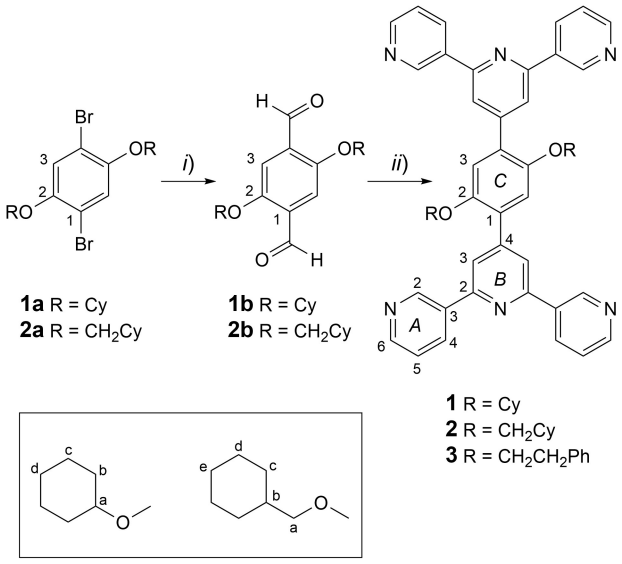

Scheme 2. Structures of ligands **1**–**3**, and the synthetic route to **1** and **2** with atom labelling for NMR spectroscopic assignments, starting from **1a** or **2a**. Reaction conditions: *i*) BuLi, Et_2O, 0 °C; DMF, 0 °C warmed to room temperature (*ca.* 22 °C); *ii*) EtOH solvent, 3-acetylpyridine, KOH, aqueous NH_3, room temperature *ca.* 22 °C.

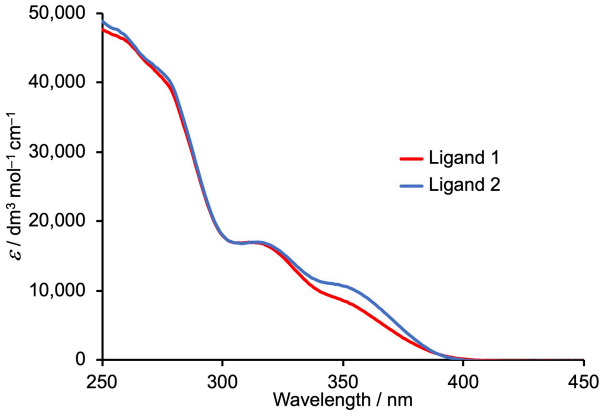

Figure 2. Solution absorption spectra ($CHCl_3$, 2.0 × 10^{-5} mol dm^{-3}) of **1** and **2**. See *Experimental Section* for values of λ_{max} and ε_{max}.

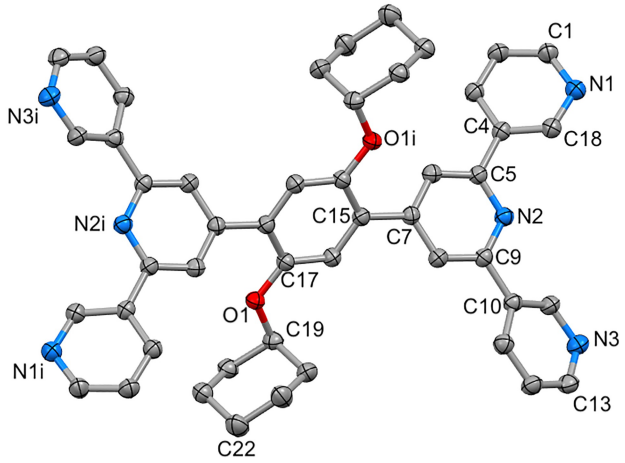

Figure 3. The structure of ligand **1** in **1**·$CHCl_3$. H-atoms and the solvent molecule are omitted for clarity; ellipsoids are plotted at 40 % probability level. Symmetry code: i = 1−*x*, 1−*y*, 1−*z*.

N2 and N3^{ii} (symmetry code ii = 1−*x*, $-^1/_2+y$, $^3/_2-z$). The angle between the planes of the rings is 5.6°, and the centroid···centroid distance is 3.65 Å, making this an efficient packing interaction.[29] This leads to the assembly of chains of molecules running parallel to the crystallographic *b*-axis (*Figure 4*).

Reactions of Co(NCS)$_2$ with Ligands **1**–**3**

Ligands **1**–**3** were reacted with cobalt(II) thiocyanate under ambient conditions by layering a methanol solution of $Co(NCS)_2$ over a chloroform, chlorobenzene or 1,2-dichlorobenzene solution of the ligand. Pink single crystals grew after around two weeks, and the reaction vessels were left to allow sufficient crystalline material to accumulate. No attempt was made to optimize yields and after crystals had been selected for single X-ray analysis, the remaining crystals were analyzed by powder X-ray diffraction (PXRD) and solid-state IR spectroscopy (see later). Combinations of $Co(NCS)_2$/**1** from MeOH/chlorobenzene, $Co(NCS)_2$/**2** from MeOH/1,2-dichlorobenzene, $Co(NCS)_2$/**3** from MeOH/1,2-dichlorobenzene, and $Co(NCS)_2$/**2** from MeOH/$CHCl_3$ produced X-ray quality crystals for which the structures are detailed below.

Crystal Structures of $[Co(NCS)_2(\mathbf{1})]_n{\cdot}2nC_6H_4Cl_2$, $[Co(NCS)_2(\mathbf{2})]_n{\cdot}4nC_6H_4Cl_2$, *and* $[Co(NCS)_2(\mathbf{3})]_n{\cdot}2.5nC_6H_5Cl$

The compounds $[Co(NCS)_2(\mathbf{1})]_n{\cdot}2nC_6H_4Cl_2$, $[Co(NCS)_2(\mathbf{2})]_n{\cdot}4nC_6H_4Cl_2$, and $[Co(NCS)_2(\mathbf{3})]_n{\cdot}2.5nC_6H_5Cl$ crystallize in the monoclinic space groups $P2_1/c$ or $P2_1/n$ (see *Experimental Section*) and the contents of the asymmetric units are displayed in *Figures S30–S32*. In each case, the asymmetric unit contains half of a bis(3,2′:6′,3″-tpy) ligand with the second half generated by inversion. The three structures are similar to one another, with the Co atom in an octahedral environment with a *trans*-arrangement of thiocyanato ligands. *Figures 5,a–5,c* illustrate that each of ligands **1**, **2** and **3** coordinates to four Co(II) centers through the outer pyridine rings of the 3,2′:6′,3″-tpy units, and atom Co1 in each structure coordinates to four different bis(3,2′:6′,3″-tpy) ligands. The Co–N bond lengths (*Table 1*) are typical. In each compound, the 3,2′:6′,3″-tpy domain adopts conformation **II** (*Scheme 1*), although note that *Scheme 1* shows limiting, planar conformations, and the angles between the planes of the pyridine rings in $[Co(NCS)_2(\mathbf{1})]_n{\cdot}2nC_6H_4Cl_2$, $[Co(NCS)_2(\mathbf{2})]_n{\cdot}4nC_6H_4Cl_2$, and $[Co(NCS)_2(\mathbf{3})]_n{\cdot}2.5nC_6H_5Cl$ range from 5.0 to 28.7° (*Table 1*). The variation in the angles is possibly a response to the different steric requirements of the R groups (Cy, CH_2Cy *versus* CH_2CH_2Ph) in ligands **1**–**3**, although the overlay of the three structures in *Figure 5,d* illustrates that the conformational changes do not have a significant impact of the directionalities of the N–Co vectors. The

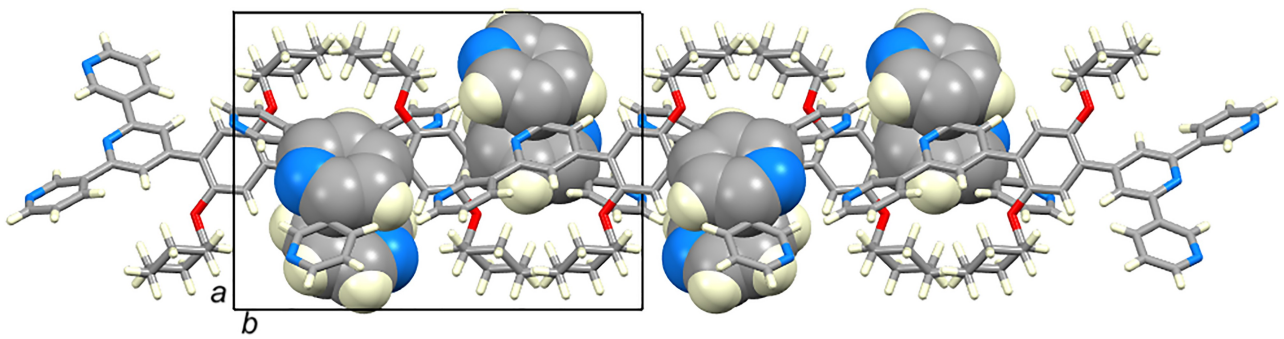

Figure 4. Molecules of **1** interact through pyridine···pyridine ring π-stacking to generate chains following the *b*-axis.

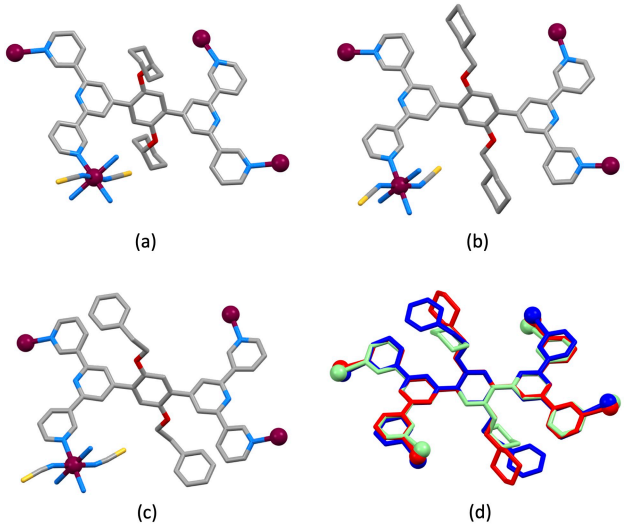

Figure 5. Ligands **1**, **2** and **3** act as 4-connecting nodes in (a) $[Co(NCS)_2(\mathbf{1})]_n{\cdot}2n C_6H_4Cl_2$, (b) $[Co(NCS)_2(\mathbf{2})]_n{\cdot}4n C_6H_4Cl_2$, and (c) $[Co(NCS)_2(\mathbf{3})]_n{\cdot}2.5n C_6H_5Cl$, respectively. H-atoms and solvent molecules are omitted for clarity. (d) An overlay of the three structural units containing ligands **1** (green), **2** (red), and **3** (blue).

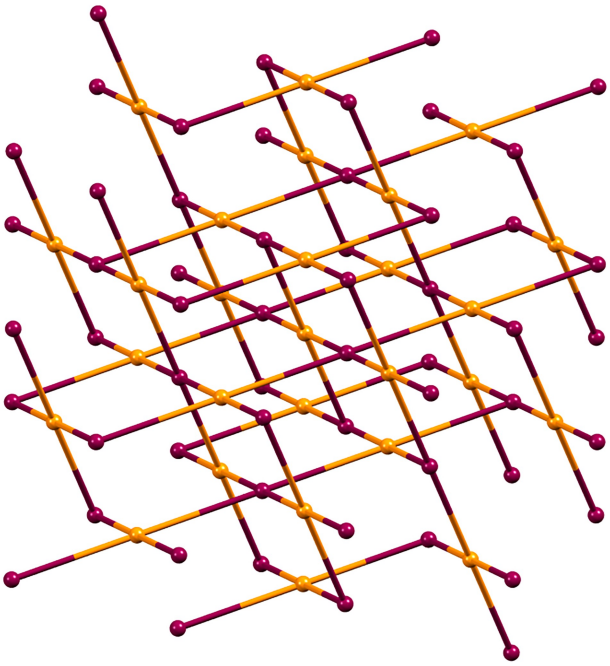

Figure 6. Part of the *cds* net in $[Co(NCS)_2(\mathbf{1})]_n{\cdot}2n C_6H_4Cl_2$ as representative of the nets in $[Co(NCS)_2(\mathbf{1})]_n{\cdot}2n C_6H_4Cl_2$, $[Co(NCS)_2(\mathbf{2})]_n{\cdot}4n C_6H_4Cl_2$, and $[Co(NCS)_2(\mathbf{3})]_n{\cdot}2.5n C_6H_5Cl$. Co and ligand nodes are shown in maroon and orange, respectively.

angles between the planes of the pyridine ring containing N2 and the arene spacer in coordinated ligands **1**, **2** and **3** are similar (*Table 1*) and are consistent with minimizing repulsive H···H interactions.

Both the cobalt(II) center and bis(3,2′:6′,3″-tpy) ligand are 4-connecting nodes, and each is essentially planar leading to the assembly of a 3-dimensional network with a *cds* topology (*Figure 6*). Thus, the networks in $[Co(NCS)_2(\mathbf{1})]_n{\cdot}2n C_6H_4Cl_2$, $[Co(NCS)_2(\mathbf{2})]_n{\cdot}4n C_6H_4Cl_2$, and $[Co(NCS)_2(\mathbf{3})]_n{\cdot}2.5n C_6H_5Cl$ follow the pattern established for solvated $[Co(NCS)_2(L)]_n$ containing bis(3,2′:6′,3″-tpy) ligands with R = propyl, butyl, pentyl, hexyl, heptyl or octyl (*Figure 1*) and in which the lattice solvent is also 1,2-dichlorobenzene.[25] In $[Co(NCS)_2(\mathbf{1})]_n{\cdot}2n C_6H_4Cl_2$, $[Co(NCS)_2(\mathbf{2})]_n{\cdot}4n C_6H_4Cl_2$, and $[Co(NCS)_2(\mathbf{3})]_n{\cdot}2.5n C_6H_5Cl$, the disordering of some of the solvent molecules makes detailed discussion of the structural roles of the

Table 1. Selected structural parameters for the cobalt(II) coordination networks.

Compound	Co–N_{NCS} [Å]	Co–N_{py} [Å]	Angle between planes of py rings containing N1/N2 and N2/N3 [°]	Angle between planes of py containing N2 and arene [°]
$[Co(NCS)_2(\mathbf{1})]_n{\cdot}2n C_6H_4Cl_2$	2.078(5)	2.154(5), 2.266(4)	9.0, 20.0	43.9
$[Co(NCS)_2(\mathbf{2})]_n{\cdot}4n C_6H_4Cl_2$	2.066(3)	2.199(3), 2.229(3)	5.0, 28.7	50.7
$[Co(NCS)_2(\mathbf{3})]_n{\cdot}2.5n C_6H_5Cl$	2.060(3)	2.168(3), 2.241(3)	15.1, 25.9	51.6
$[Co_2(NCS)_4(\mathbf{2})_2]_n{\cdot}5.5n CHCl_3{\cdot}0.2n MeOH$	2.080(5) (for Co1), 2.091(6) (for Co2)	2.187(4), 2.257(4) (for Co1) 2.147(5), 2.150(4) (for Co2)	9.3, 16.4[a] 31.0, 35.5[b]	46.7[a] 34.3[b]

[a] For the tpy unit containing N1 N2 N3. [b] Tpy unit containing N4 N5 N6.

solvent molecules difficult. In $[Co(NCS)_2(\mathbf{2})]_n{\cdot}4nC_6H_4Cl_2$, one 1,2-dichlorobenzene molecule is ordered, while the second is disordered and was modelled over two sites of occupancies of 70 and 30%. The ordered $C_6H_4Cl_2$ molecule lies over the pyridine ring containing N2, with a centroid···centroid distance of 4.1 Å and inter-plane angle of 9.5°, leading to a weak face-to-face π-stacking interaction. In $[Co(NCS)_2(\mathbf{1})]_n{\cdot}2nC_6H_4Cl_2$, the disordered 1,2-dichlorobenzene molecule was modelled over three sites of occupancies 20, 30 and 50%; however, there is evidence for face-to-face stacking with the pyridine ring containing N2. Although the structure of $[Co(NCS)_2(\mathbf{3})]_n{\cdot}2.5nC_6H_5Cl$ suffers significant disorder, both in the solvent molecules and phenylethyl group (see the caption to *Figure S32*), there is evidence once again for face-to-face stacking between the central pyridine ring of the tpy unit and a chlorobenzene molecule. However, these are not the sole packing interactions involving the solvent molecules. It is relevant to consider that the unsolvated *cds* networks in $[Co(NCS)_2(\mathbf{1})]_n$, $[Co(NCS)_2(\mathbf{2})]_n$, and $[Co(NCS)_2(\mathbf{3})]_n$ have large voids. Using a probe radius of 1.2 Å, the voids were calculated in Mercury 2022.2.0[30] to be *ca.* 40% in each of the structures with ligands **1** and **2**; the void space in $[Co(NCS)_2(\mathbf{3})]_n$ is also large, but we have not quantified it because of the disordered phenylethyl substituents.

Figure 7 shows the $[Co(NCS)_2(\mathbf{1})]_n$ network and the manner in which the 1,2-dichlorobenzene molecules occupy the channels; although the cyclohexyl substituents point into the channels, the remaining solvent accessible void remains large, and the dimensions of the aromatic solvent molecules match well to those of the channels.

Crystal Structure of $[Co_2(NCS)_4(\mathbf{2})_2]_n{\cdot}5.5nCHCl_3{\cdot}0.2nMeOH$

With a change in the crystallization solvent system from MeOH/C_6H_5Cl or MeOH/1,2-$C_6H_4Cl_2$ to MeOH/$CHCl_3$, it was possible to isolate single crystals of $[Co_2(NCS)_4(\mathbf{2})_2]_n{\cdot}5.5nCHCl_3{\cdot}0.2nMeOH$. The compound crystallizes in the monoclinic space group *C*2/*c*, and the asymmetric unit contains two independent half-molecules of **2**, both second halves being generated across inversion centers. The crystallographically independent cobalt atoms, Co1 and Co2 are both octahedrally sited and are coordinated by *trans*-NCS^- ligands and the N-donors of four different ligands **2**. Selected bond lengths and inter-ring angles are given in *Table 1*. Each bis(3,2′:6′,3″-tpy) ligand coordinates to two Co1 and two Co2 atoms, and both crystallographically independent 3,2′:6′,3″-tpy units adopt conformation **II** (*Scheme 1*). Thus, the local environments of ligand **2**, Co1 and Co2

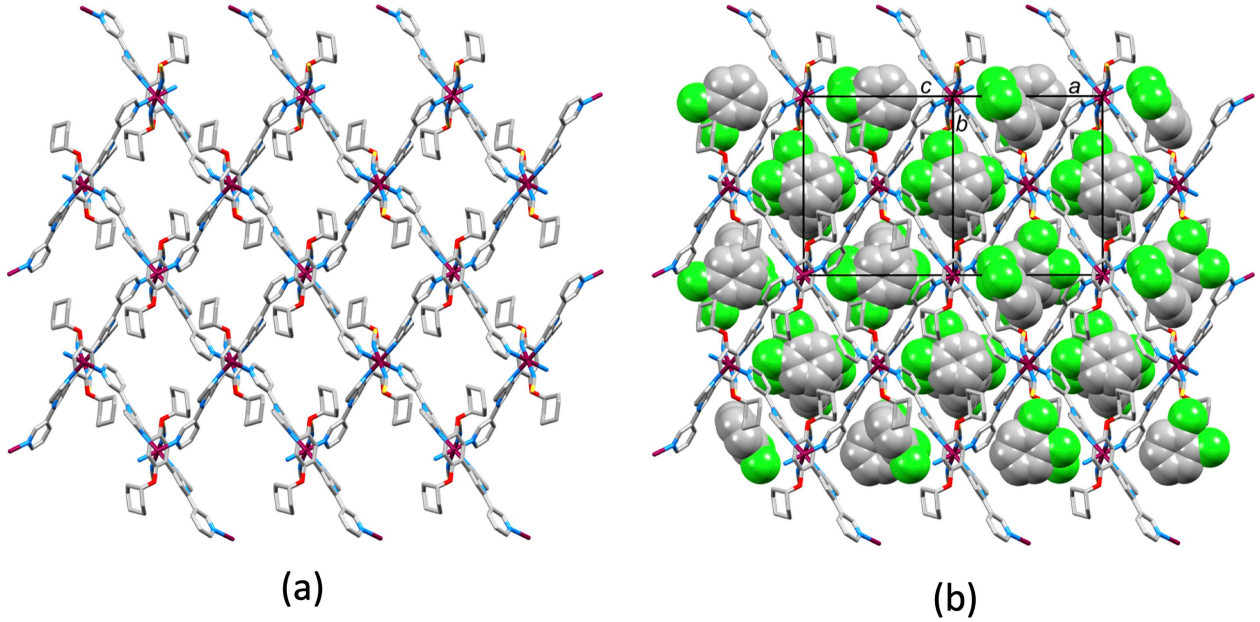

Figure 7. Part of the network in $[Co(NCS)_2(\mathbf{1})]_n{\cdot}2nC_6H_4Cl_2$ (a) without and (b) with solvent molecules (shown in space-filling representation).

(*Figure 8*) mimic those of the ligands and metal centers in $[Co(NCS)_2(\mathbf{1})]_n{\cdot}2n C_6H_4Cl_2$, $[Co(NCS)_2(\mathbf{2})]_n{\cdot}4n C_6H_4Cl_2$, and $[Co(NCS)_2(\mathbf{3})]_n{\cdot}2.5n C_6H_5Cl$. However, in

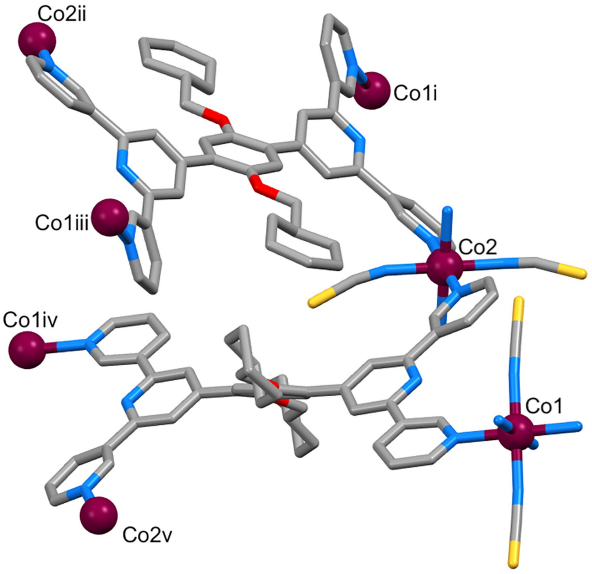

Figure 8. Repeating unit in $[Co_2(NCS)_4(\mathbf{2})_2]_n{\cdot}5.5n CHCl_3{\cdot}0.2n MeOH$; H-atoms and solvent molecules are omitted and symmetry generated Co atoms are labelled: symmetry codes i = 1−*x*, 1+*y*, $^1/_2-z$; ii = $^3/_2-x$, $^3/_2-y$, 1−*z*; iii = $^3/_2-x$, $^1/_2+y$, $^1/_2-z$; iv = $^1/_2+x$, $^1/_2+y$, 1+*z*; v = $^3/_2-x$, $^1/_2-y$, 1−*z*. See *Figure S33* for additional atom labels.

$[Co_2(NCS)_4(\mathbf{2})_2]_n{\cdot}5.5n CHCl_3{\cdot}0.2n MeOH$, the combination of four chemically distinct planar, 4-connecting nodes defined by Co1, Co2 and the centroids of the two independent phenylene rings results in the assembly of a complex 3-dimensional network. Since the two ligand nodes are topologically equivalent (as described in our previous work[24]), the net is trinodal. The network is self-penetrating as shown in *Figure 9* and is analogous to that found in $[Co(NCS)_2(L_1)]_n{\cdot}n MeOH{\cdot}3n CHCl_3$ and $[Co(NCS)_2(L_2)]_n{\cdot}0.8n MeOH{\cdot}1.8n CHCl_3$ where ligands L_1 and L_2 are in the family defined in *Figure 1* with R = 2-ethylbutyl and 3-methylbutyl, respectively.[24]

Combinations of $Co(NCS)_2$/**1** and $Co(NCS)_2$/**3** from $MeOH/CHCl_3$ gave rise to crystals for which only preliminary structural data could be obtained. However, in both cases, the data confirmed the assembly of trinodal self-interpenetrating networks analogous to that found for $[Co_2(NCS)_4(\mathbf{2})_2]_n{\cdot}5.5n CHCl_3{\cdot}0.2n MeOH$. As in the structures described in the previous section, the void space in the non-solvated $[Co_2(NCS)_4(\mathbf{2})_2]_n$ lattice is large (*ca.* 34%, calculated using a probe radius of 1.2 Å with Mercury 2022.2.0[30]). The persistence of the trinodal self-interpenetrating net when the crystallization solvent mixture is $MeOH/CHCl_3$ and the absence of the *cds* net under these crystallization conditions suggests that the cavities accessible to solvent in the trinodal self-interpenetrating net are compatible with the relatively small

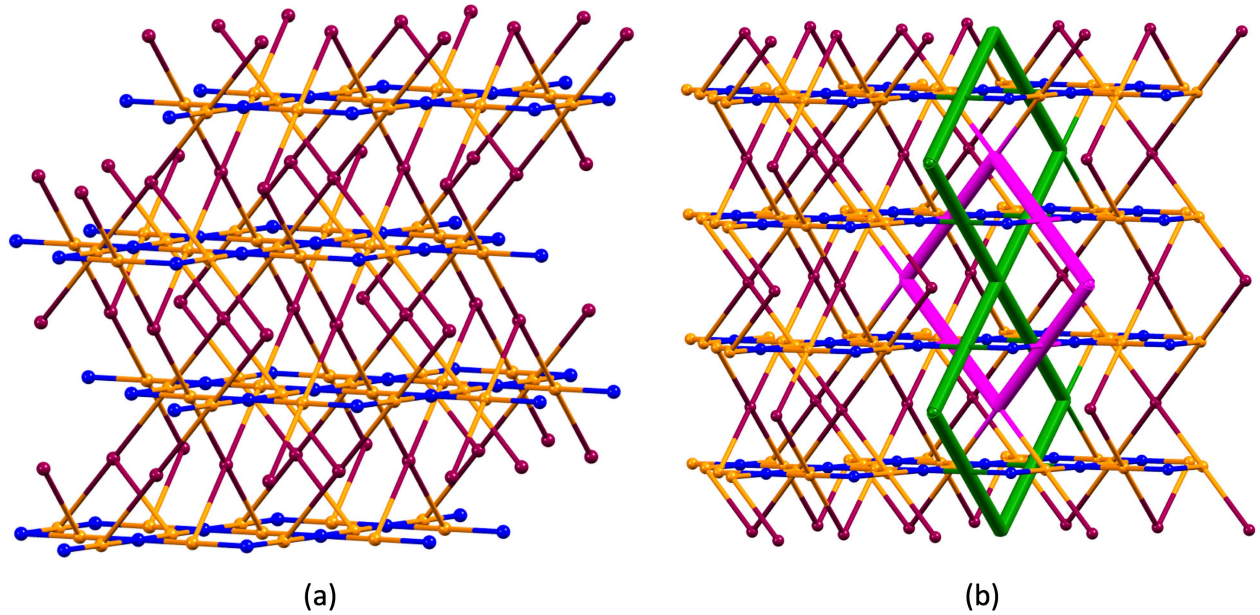

Figure 9. (a) Part of the trinodal $(6^2.8^4)(6^4.8^2)(6^5.8)_2$ net in $[Co_2(NCS)_4(\mathbf{2})_2]_n{\cdot}5.5n CHCl_3{\cdot}0.2n MeOH$ with the Co1 nodes shown in maroon, Co2 nodes in blue, and ligand centroid nodes in orange. (b) Part of the lattice showing self-penetration defined by the interlocking of the shortest circuits shown in green and magenta.

$CHCl_3$ and MeOH molecules, but not chlorobenzene or 1,2-dichlorobenzene.

Bulk Material Characterization

After selection of single crystals for structure determination, the remaining crystals in each reaction tube were analyzed by solid-state IR spectroscopy and powder X-ray diffraction. *Figures S34–S37* display the IR spectra of $[Co(NCS)_2(\mathbf{1})]_n{\cdot}2n C_6H_4Cl_2$, $[Co(NCS)_2(\mathbf{2})]_n{\cdot}4n C_6H_4Cl_2$, $[Co(NCS)_2(\mathbf{3})]_n{\cdot}2.5n C_6H_5Cl$ and $[Co_2(NCS)_4(\mathbf{2})_2]_n{\cdot}5.5n CHCl_3{\cdot}0.2n MeOH$, respectively. The complexes containing ligands **1** or **2** give rise to IR absorptions around 2930 cm^{-1} which resemble those in the free ligands (compare *Figures S34*, *S35* and *S38* with *Figures S28* and *S29*) and are assigned to the cyclohexyl groups. The coordinated NCS^- ligands lead to very strong absorptions (ν_{CN}) at 2056 cm^{-1} in $[Co(NCS)_2(\mathbf{1})]_n{\cdot}2n C_6H_4Cl_2$ (*Figure S34*), 2064 cm^{-1} in $[Co(NCS)_2(\mathbf{2})]_n{\cdot}4n C_6H_4Cl_2$ (*Figure S37*), 2054 cm^{-1} in $[Co(NCS)_2(\mathbf{3})]_n{\cdot}2.5n C_6H_5Cl$ (*Figure S36*), and 2064 cm^{-1} in $[Co_2(NCS)_4(\mathbf{2})_2]_n{\cdot}5.5n CHCl_3{\cdot}0.2n MeOH$ (*Figure S35*).

PXRD data for the bulk material for $[Co(NCS)_2(\mathbf{1})]_n{\cdot}2n C_6H_4Cl_2$ and $[Co(NCS)_2(\mathbf{3})]_n{\cdot}2.5n C_6H_5Cl$ revealed excellent fits between the experimental PXRD patterns and those predicted from the single-crystal structures (*Figure 10,a* and *10,c*), thus confirming that the *cds* coordination nets observed in each single crystal structure represented the bulk material. For $[Co(NCS)_2(\mathbf{2})]_n{\cdot}4n C_6H_4Cl_2$, the experimental powder pattern contains all the predicted peaks, but there are additional peaks present at low values of 2θ (*Figure 10,b*) indicating the presence of at least one other species in the bulk material. Crystals of $[Co_2(NCS)_4(\mathbf{2})_2]_n{\cdot}5.5n CHCl_3{\cdot}0.2n MeOH$ were extremely sensitive to solvent loss and it was not possible to obtain a PXRD pattern that was consistent with the predicted pattern from the single crystal structure.

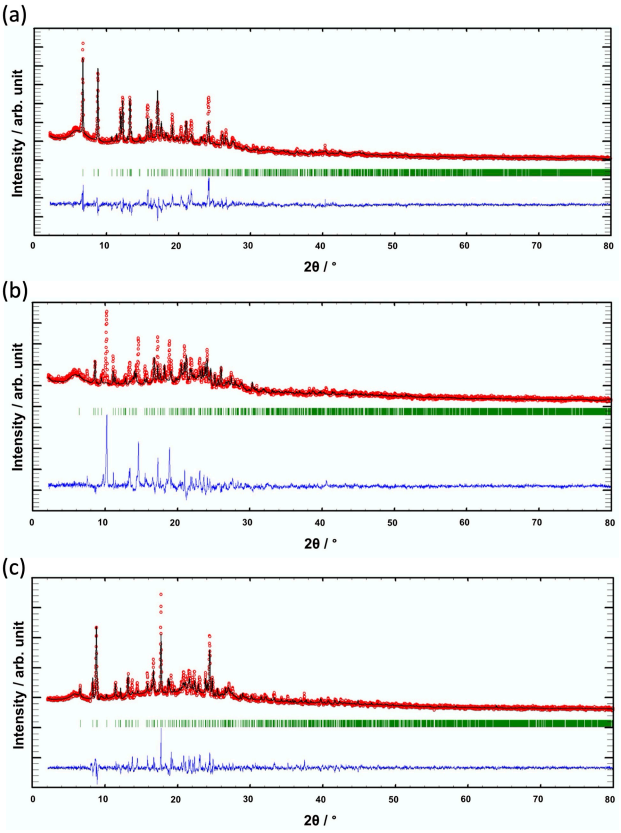

Figure 10. PXRD (CuKα1 radiation) patterns for (a) $[Co(NCS)_2(\mathbf{1})]_n{\cdot}2n C_6H_4Cl_2$, (b) $[Co(NCS)_2(\mathbf{2})]_n{\cdot}4n C_6H_4Cl_2$, and (c) $[Co(NCS)_2(\mathbf{3})]_n{\cdot}2.5n C_6H_5Cl$. Each experimentally obtained pattern (red) is compared with the best fit from the *Rietveld* refinement analysis (black). *Bragg* peak positions (green) and differences between the calculated and experimental plots (blue) are also displayed.

Conclusions

The bis(3,2′:6′,3′′-tpy) ligands **1**, **2** and **3** act as 4-connecting nodes and react with $Co(NCS)_2$ under conditions of crystal growth by layering at room temperature to produce 3-dimensional nets with either a *cds* or trinodal self-penetrating topology. Both these nets contain planar, 4-connecting metal and ligand nodes. The choice of solvents ($MeOH/C_6H_5Cl$, $MeOH/1,2\text{-}Cl_2C_6H_5$, or $MeOH/CHCl_3$) used in the crystallization experiments is critical, with the aromatic solvents occupying channels in the *cds* nets found for $[Co(NCS)_2(\mathbf{1})]_n{\cdot}2n C_6H_4Cl_2$, $[Co(NCS)_2(\mathbf{2})]_n{\cdot}4n C_6H_4Cl_2$, and $[Co(NCS)_2(\mathbf{3})]_n{\cdot}2.5n C_6H_5Cl$. In contrast, the smaller $CHCl_3$ and MeOH molecules are accommodated in cavities in the trinodal self-penetrating net in $[Co_2(NCS)_4(\mathbf{2})_2]_n{\cdot}5.5n CHCl_3{\cdot}0.2n MeOH$. Preliminary structural data for single crystals grown by layering a MeOH solution of $Co(NCS)_2$ over a $CHCl_3$ solution of **1** or **3** confirmed the assemblies of trinodal self-penetrating nets in both products. PXRD data for the bulk materials of $[Co(NCS)_2(\mathbf{1})]_n{\cdot}2n C_6H_4Cl_2$ and $[Co(NCS)_2(\mathbf{3})]_n{\cdot}2.5n C_6H_5Cl$ confirm that the single crystal structures are representative of the bulk sample; solvent loss from crystals of $[Co_2(NCS)_4(\mathbf{2})_2]_n{\cdot}5.5n CHCl_3{\cdot}0.2n MeOH$ contributed to the poor match between experimental and predicted powder patterns. The solvent-dependent, selective assembly of either a *cds* or trinodal self-penetrating 3-dimensional network in reactions of $Co(NCS)_2$ with **1**, **2**

and **3** is consistent with our previous results using different 1,4-bis(alkyloxy)-2,5-bis(3,2′:6′,3″-terpyridin-4′-yl)benzene ligands.[24,25]

Experimental Section

General

^{1}H- and ^{13}C{^{1}H}-NMR spectra were recorded on a *Bruker Avance III-500* spectrometer equipped with a BBFO probe head at 298 K. The ^{1}H- and ^{13}C-NMR chemical shifts were referenced with respect to residual solvent peaks (δ 7.26 ppm for $CHCl_3$ and δ 77.2 ppm for $CDCl_3$, respectively with δ TMS = 0). Matrix-assisted laser desorption ionization time-of-flight (MALDI-TOF) mass spectra were recorded on a *Shimadzu MALDI 8020* instrument using α-cyano-4-hydroxycinnamic acid (CHCA) or 2,5-dihydroxybenzoic acid as the matrix as detailed in the captions to figures in the *Supporting Information*. *PerkinElmer UATR Two* and *Shimadzu UV-2600* instruments were used to record FT-IR and UV-Vis absorption spectra, respectively. Melting points were determined using a *Stuart* melting point *SMP 30* device. Elemental analyses and high-resolution electrospray (HR-ESI) mass spectra were performed using a *Vario MICRO Cube* device and *Bruker maXis 4G QTOF* instrument, respectively. Analytical thin-layer chromatography was conducted with pre-coated silica gel *60* F_{254} aluminum sheets (*Merck KGaA*) and visualized using UV light (254 nm and 366 nm). Flash column chromatography was performed on a *Biotage Selekt* system with pre-packed silica gel columns (50 g *Biotage Sfär Silica High Capacity Duo 20* μm) using ethyl acetate in cyclohexane (gradient) as eluent and monitoring and collecting at 366 nm.

3-Acetylpyridine and cyclohexyl bromide were purchased from *Acros Organics* and [$Co(NCS)_2$] from *Alfa Aesar*, and (bromomethyl)cyclohexane and 2,5-dibromobenzene-1,4-diol were from *Fluorochem*. Crystal growth experiments were carried out under ambient conditions using glass test-tubes (i.d. = 13.6 mm, 24 mL). Ligand **3** was prepared according to a previously reported method.[26]

Compound **1a**

2,5-Dibromohydroquinone (4.00 g, 14.9 mmol, 1.0 equiv.), bromocyclohexane (15.6 mL, 127 mmol, 8.5 equiv.) and anhydrous K_2CO_3 (17.51 g, 126.7 mmol, 8.5 equiv.) were combined in dry DMF (100 mL) and the mixture was heated to 100 °C and stirred for 48 h under N_2. The mixture was then allowed to cool to room temperature, poured onto ice water (200 mL) and stirred for 20 min. The resulting suspension was extracted with chloroform (3 × 150 mL). The organic layers were combined, dried over $MgSO_4$ and concentrated *in vacuo*. The crude product was purified by column chromatography (silica, 100% dichloromethane) yielding **1a** (910 mg, 2.10 mmol, 14.1%) as off-white crystals. M.p. 92.8–95.6 °C. ^{1}H-NMR (500 MHz, $CDCl_3$): 7.11 (*s*, 2 H, H^3); 4.16 (*tt*, J = 8.3, 3.7, 2 H, H^a); 1.96–1.88 (*m*, 4 H, H^{b-eq}); 1.85–1.77 (*m*, 4 H, H^{c-eq}); 1.65–1.57 (*m*, 4 H, H^{b-ax}); 1.57–1.50 (*m*, 2 H, H^{d-eq}); 1.41–1.30 (*m*, 6 H, $H^{c-ax+d-ax}$). ^{13}C-NMR (126 MHz, $CDCl_3$): 149.3 (C^2); 121.4 (C^3); 113.0 (C^1); 78.5 (C^a); 31.7 (C^b); 25.7 (C^d); 23.6 (C^c). UV-Vis ($CHCl_3$, 6×10^{-5} mol dm^{-3}): 302 (ε/dm^3 mol^{-1} cm^{-1} 4,170). Anal. calc. for $C_{18}H_{24}Br_2O_2$: C 50.02, H 5.60; found: C 50.34, H 5.64.

Compound **2a**

2,5-Dibromohydroquinone (2.50 g, 9.33 mmol, 1.0 equiv.), (bromomethyl)cyclohexane (4.6 mL, 33 mmol, 3.5 equiv.) and anhydrous K_2CO_3 (4.50 g, 32.6 mmol, 3.5 equiv.) were combined in dry DMF (100 mL) and the mixture was heated to 100 °C and stirred for 16 h under N_2. The mixture was then allowed to cool to room temperature, poured onto ice water (150 mL) and was stirred for 20 min. The resulting suspension was extracted with chloroform (3 × 150 mL). The organic layers were combined, dried over $MgSO_4$ and concentrated *in vacuo*. The crude product was reprecipitated under gentle stirring from a hot EtOH (25 mL) and chloroform (15 mL) solution over 16 h. The resultant precipitate was collected by filtration, washed with EtOH and dried *in vacuo* to yield **2a** (2.43 g, 5.28 mmol, 56.7%) as a white solid. M.p. 130.0–132.7 °C. ^{1}H-NMR (500 MHz, $CDCl_3$): 7.06 (*s*, 2 H, H^3); 3.74 (*d*, J = 6.3, 4 H, H^a); 1.92–1.86 (*m*, 4 H, H^{c-eq}); 1.86–1.80 (*m*, 2 H, H^b); 1.80–1.73 (*m*, 4 H, H^{d-eq}); 1.74–1.67 (*m*, 2 H, H^{e-eq}); 1.30 (*qt*, J = 12.5, 3.3, 4 H, H^{d-ax}); 1.20 (*qt*, J = 12.7, 3.2, 2 H, H^{e-ax}); 1.14–1.02 (*m*, 4 H, H^{c-ax}). ^{13}C-NMR (126 MHz, $CDCl_3$): 150.3 (C^2); 118.5 (C^3); 111.2 (C^1); 75.8 (C^a); 37.8 (C^b); 29.9 (C^c); 26.6 (C^e); 25.9 (C^d). UV-Vis ($CHCl_3$, 6×10^{-5} mol dm^{-3}): 302 (ε/dm^3 mol^{-1} cm^{-1} 5,060). Anal. calc. for $C_{20}H_{28}Br_2O_2$: C 52.19, H 6.13; found: C 52.21, H 6.18.

Compound **1b**

Compound **1a** (800 mg, 1.85 mmol, 1.0 equiv.) was dissolved in dry Et_2O (30 mL), and the solution was cooled to 0 °C under N_2. BuLi (15% in hexanes, 1.6 M, 4.6 mL, 7.4 mmol, 4.0 equiv.) was added at 0 °C over a period of 15 min, and the mixture was stirred at 0 °C for 2 h. Dry DMF (580 µL, 7.4 mmol, 4.0 equiv.) was added, and the mixture was stirred for 16 h, allowing the mixture to slowly warm from 0 °C to room temperature. The now light yellow suspension was quenched by the addition of saturated aqueous NH_4Cl (100 mL) and subsequently extracted with chloroform (3× 100 mL). The organic layers were combined, dried over $MgSO_4$ and concentrated *in vacuo*. The crude material was purified by column chromatography (silica, AcOEt in cyclohexane 0–10% gradient). After the removal of solvent from the fractions collected, the yellow solid was recrystallized from a hot solution of petroleum ether (5 mL) and EtOH (5 mL). The yellow solution was allowed to slowly cool to −20 °C and was left to crystallize for 48 h. The resultant crystals were collected by filtration, washed with petroleum ether and dried *in vacuo* to give **1b** (129 mg, 390 µmol, 21.1%) as a yellow crystalline solid. M.p. 109.4–111.4 °C. ^{1}H-NMR (500 MHz, $CDCl_3$): 10.52 (*s*, 2 H, H^{CHO}); 7.43 (*s*, 2 H, H^3); 4.42 (*tt*, J = 8.3, 3.7, 2 H, H^a); 2.01–1.94 (*m*, 4 H, H^{b-eq}); 1.84–1.73 (*m*, 4 H, H^{c-eq}); 1.67–1.55 (*m*, 6 H, $H^{b-ax+d-eq}$); 1.50–1.29 (*m*, 6 H, $H^{c-ax+d-ax}$). ^{13}C-NMR (126 MHz, $CDCl_3$): 190.0 (C^{CHO}); 154.1 (C^2); 130.6(C^1); 113.7 (C^3); 77.4 (C^a); 31.7 (C^b); 25.6 (C^d); 23.6 (C^c). UV-Vis ($CHCl_3$, 2×10^{-5} mol dm^{-3}): 275 (ε/dm^3 mol^{-1} cm^{-1} 14,400), 283 sh (12,170), 408 (5,050). MALDI-TOF-MS: 331.29 ([M+H]$^+$; calc. 331.19). Anal. calc. for $C_{20}H_{26}O_4$: C 72.70, H 7.93; found: C 72.85, H 8.12.

Compound **2b**

Compound **2a** (2.00 g, 4.34 mmol, 1.0 equiv.) was dissolved in dry Et_2O (80 mL), and the solution was cooled to 0 °C under N_2. BuLi (15% in hexanes, 1.6 M, 10.9 mL, 17.4 mmol, 4.0 equiv.) was added at 0 °C over a period of 15 min, and the mixture was stirred at 0 °C for 2 h. Dry DMF (1.4 mL, 17 mmol, 4.0 equiv.) was added, and the mixture was stirred for 16 h, allowing the mixture to slowly warm from 0 °C to room temperature. The now light yellow suspension was quenched by the addition of saturated aqueous NH_4Cl (100 mL) and subsequently extracted with chloroform (3× 100 mL). The organic layers were combined, dried over $MgSO_4$ and concentrated *in vacuo*. The crude material was purified by column chromatography (silica, AcOEt in cyclohexane 0–10% gradient). After the removal of solvent from the fractions collected, the yellow solid was recrystallized from a hot solution of petroleum ether (15 mL) and AcOEt (5 mL). The yellow solution was allowed to cool slowly to room temperature and was left to crystallize for 16 h. The resultant crystals were collected by filtration, washed with petroleum ether and dried *in vacuo* to give **2b** (530 mg, 1.48 mmol, 34.1%) as a yellow crystalline solid. M.p. 141.3–143.6 °C. ^{1}H-NMR (500 MHz, $CDCl_3$): 10.53 (*s*, 2 H, H^{CHO}); 7.41 (*s*, 2 H, H^3); 3.88 (*d*, J = 5.9, 4 H, H^a); 1.90–1.82 (*m*, 6 H, H^{b+c-eq}); 1.78 (*ddd*, J = 13.8, 4.4, 2.3, 4 H, H^{d-eq}); 1.74–1.67 (*m*, 2 H, H^{e-eq}); 1.31 (*qt*, J = 12.5, 3.1, 4 H, H^{d-ax}); 1.25–1.16 (*m*, 2 H, H^{e-ax}); 1.14–1.04 (*m*, 4 H, H^{c-ax}). ^{13}C-NMR (126 MHz, $CDCl_3$): 189.6 (C^{CHO}); 155.5 (C^2); 129.5 (C^1); 111.7 (C^3); 74.7 (C^a); 37.8 (C^b); 30.0 (C^c); 26.5 (C^e); 25.9 (C^d). UV-Vis ($CHCl_3$, 2×10^{-5} mol dm^{-3}): 275 (ε/dm^3 mol^{-1} cm^{-1} 14,980), 283 sh (12,620), 406 (5,840). MALDI-TOF-MS: 359.07 ([M+H]$^+$; calc. 359.22). Anal. calc. for $C_{22}H_{30}O_4$: C 73.71, H 8.44; found: C 73.84, H 8.65.

Compound **1**

Compound **1b** (100 mg, 303 µmol, 1.0 equiv.) was dissolved at room temperature in EtOH (5 mL). 3-Acetylpyridine (170 µL, 1.5 mmol, 5.0 equiv.) and crushed KOH (85 mg, 1.5 mmol, 5.0 equiv.) were then added to the yellow solution and slow addition of aqueous NH_3 (32%, 4.4 mL) followed. The mixture turned over a dark red into an orange suspension and was stirred at room temperature for 7 d. The solid that formed was collected by filtration, washed with H_2O (3×5 mL) followed by EtOH (3×5 mL) and dried *in vacuo*. The title compound **1** was isolated as a light-brown solid (109 mg, 147 µmol, 48.6%). Decomposition >262 °C. ^{1}H-NMR (500 MHz, $CDCl_3$): 9.39 (*d*, J = 2.3, 4 H, H^{A2}); 8.72 (*dd*, J = 4.8, 1.7, 4 H, H^{A6}); 8.56 (*dt*, J = 8.0, 2.0, 4 H, H^{A4}); 8.05 (*s*, 4 H, H^{B3}); 7.50 (*dd*, J = 8.0, 4.8, 4 H, H^{A5}); 7.17 (*s*, 2 H, H^{C3}); 4.29 (*tt*, J = 8.2, 3.6, 2 H, H^a); 1.97–1.87 (*m*, 4 H, H^{b-eq}); 1.72–1.61 (*m*, 4 H, H^{c-eq}); 1.59–1.43 (*m*, 6 H, $H^{b-ax+d-eq}$); 1.38–1.16 (*m*, 6 H, $H^{c-ax+d-ax}$). ^{13}C-NMR (126 MHz, CDCl3): 154.7 (C^{B2}); 150.1 (C^{A6}); 149.3 (C^{C2}); 148.4 (C^{C1}); 148.3 (C^{A2}); 135.0 (C^{A3}); 134.8 (C^{A4}); 130.7 (C^{B4}); 123.9 (C^{A5}); 120.4 (C^{B3}); 117.9 (C^{C3}); 77.4 (C^a); 31.9 (C^b); 25.5 (C^d); 23.5 (C^c). UV-Vis ($CHCl_3$, 1×10^{-5} mol dm^{-3}): 261 sh (ε/dm^3 mol^{-1} cm^{-1} 45,820), 277 sh (39,770), 313 (16,950), 354 sh (8,010). MALDI-TOF-MS: 737.11 ([M+H]$^+$; calc. 737.36). HR-ESI MS: 737.3589 ([M+H]$^+$; calc. 737.3599). Sat-

isfactory elemental analytical data could not be obtained.

Compound **2**

Compound **2b** (500 mg, 1.39 mmol, 1.0 equiv.) was dissolved at room temperature in EtOH (20 mL). 3-Acetylpyridine (770 µL, 7.0 mmol, 5.0 equiv.) and crushed KOH (390 mg, 7.0 mmol, 5.0 equiv.) were then added to the yellow solution and slow addition of aqueous NH_3 (32 %, 20 mL) followed. The mixture turned over a dark red into an orange suspension and was stirred at room temperature for 3 d. The solid that formed was collected by filtration, washed with H_2O (3×10 mL) followed by EtOH (3×10 mL) and dried *in vacuo*. The crude product was recrystallized from a hot solution of EtOH (5 mL) and $CHCl_3$ (1 mL). The solution was allowed to cool slowly to room temperature and was left to crystallize for 16 h. The resultant crystals were collected by filtration, washed with EtOH and dried *in vacuo* to give **2** (291 mg, 380 µmol, 27.4 %) as an off-white crystalline solid. M.p. 252.9–254.9 °C. ^{1}H-NMR (500 MHz, $CDCl_3$): 9.39 (*dd*, *J* = 2.4, 0.9, 4 H, H^{A2}); 8.72 (*dd*, *J* = 4.9, 1.7, 4 H, H^{A6}); 8.57 (*dt*, *J* = 8.1, 1.9, 4 H, H^{A4}); 8.05 (*s*, 4 H, H^{B3}); 7.51 (*ddd*, *J* = 8.0, 4.8, 0.9, 4 H, H^{A5}); 7.15 (*s*, 2 H, H^{C3}); 3.86 (*d*, *J* = 5.8, 4 H, H^{a}); 1.77 (*tq*, *J* = 10.0, 6.2, 4.5, 6 H, $H^{b\,+\,c-eq}$); 1.62 (*td*, *J* = 16.2, 14.8, 8.6, 6 H, $H^{d-eq\,+\,e-eq}$); 1.17 (*qt*, *J* = 13.7, 3.6, 4 H, H^{d-ax}); 1.10–0.94 (*m*, 6 H, $H^{c-ax\,+\,e-ax}$). ^{13}C-NMR (126 MHz, $CDCl_3$): 154.7 (C^{B2}); 150.8 (C^{C2}); 149.9 (C^{A6}); 148.2 (C^{C1}); 148.1 (C^{A2}); 135.02 (C^{A3}); 134.97 (C^{A4}); 129.3 (C^{B4}); 123.9 (C^{A5}); 120.5 (C^{B3}); 115.1 (C^{C3}); 75.1 (C^{a}); 38.1 (C^{b}); 30.1 (C^{c}); 26.4 (C^{e}); 25.8 (C^{d}). UV-Vis ($CHCl_3$, 1×10^{-5} mol dm^{-3}): 260 sh (ε/dm^3 mol^{-1} cm^{-1} 46,260), 277 sh (40,540), 315 (16,960), 354 sh (10,220). MALDI-TOF-MS: 765.20 ($[M+H]^+$; calc. 765.39). HR-ESI MS: 765.3896 ($[M+H]^+$; calc. 765.3912). Satisfactory elemental analytical data could not be obtained.

$[Co(NCS)_2(\mathbf{1})]_n \cdot 2n C_6H_4Cl_2$

A MeOH (5 mL) solution of $Co(NCS)_2$ (1.8 mg, 10 µmol) was layered over a 1,2-dichlorobenzene solution (4 mL) of ligand **1** (7.4 mg, 10 µmol). Pink block-shaped crystals grew after 22 d. A single crystal was selected for X-ray diffraction and the remaining crystals were analyzed by PXRD and FT-IR spectroscopy.

$[Co(NCS)_2(\mathbf{2})]_n \cdot 4n C_6H_4Cl_2$

A MeOH (5 mL) solution of $Co(NCS)_2$ (1.8 mg, 10 µmol) was layered over a 1,2-dichlorobenzene solution (4 mL) of ligand **2** (7.7 mg, 10 µmol). Pink block-shaped crystals grew after 15 d. A single crystal was selected for X-ray diffraction and the remaining crystals were analyzed by PXRD and FT-IR spectroscopy.

$[Co_2(NCS)_4(\mathbf{2})_2]_n \cdot 5.5n CHCl_3 \cdot 0.2n MeOH$

A MeOH (5 mL) solution of $Co(NCS)_2$ (1.8 mg, 10 µmol) was layered over a chloroform solution (4 mL) of ligand **2** (7.7 mg, 10 µmol). Orange block-shaped crystals grew after 15 d. A single crystal was selected for X-ray diffraction and the remaining crystals were analyzed by PXRD and FT-IR spectroscopy.

$[Co(NCS)_2(\mathbf{3})]_n \cdot 2.5n C_6H_5Cl$

A MeOH (8 mL) solution of $Co(NCS)_2$ (1.8 mg, 10 µmol) was layered over a chlorobenzene solution (5 mL) of ligand **3** (7.8 mg, 10 µmol). Pink block-like crystals visible to the eye were first obtained after 17 d, and a single crystal was selected for X-ray diffraction. The remaining crystals were analyzed by powder X-ray diffraction and FT-IR spectroscopy.

Crystallography

Single crystal data were collected on a *STOE StadiVari Eulerian 4-circle* diffractometer (CuKα radiation) equipped with a *Dectris Eiger2 1 M* detector, or using a *STOE StadiVari* diffractometer equipped with a *Pilatus300 K* detector and with a *Metaljet D2* source (GaKα radiation) with data processing using STOE software (X-Area 1.90, STOE, 2020). Structures were solved using Superflip[31,32] and Olex2.[33] The model was refined with ShelXL v. 2018/3.[34] All H atoms were included at geometrically calculated positions and refined using a riding model with $U_{iso} = 1.2$ of the parent atom. Structure analysis and structural diagrams used CSD Mercury 2022.2.0.[30]

In some structures, the S-atom of the $[NCS]^-$ unit and the cyclohexyl or phenylethyl substituent suffered from disorder, and details of the treatment of the disorders and site occupancies are given in the *Supporting Information* in the relevant figure captions. In $[Co(NCS)_2(\mathbf{1})]_n \cdot 2n C_6H_4Cl_2$ and $[Co(NCS)_2(\mathbf{3})]_n \cdot 2.5n C_6H_5Cl$ geometrical restraints for the aromatic ring and restraints for their thermal parame-

ters had to be used to treat the disordered 1,2-dichlorobenzene molecules, chlorobenzene respectively, in the modelling process. The cyclohexyl substituent in $[Co(NCS)_2(\mathbf{1})]_n{\cdot}2nC_6H_4Cl_2$ showed large thermal motion requiring restraints for the thermal parameter. A solvent mask was applied to treat part of the solvent region in $[Co_2(NCS)_4(\mathbf{2})_2]_n{\cdot}5.5nCHCl_3{\cdot}0.2n$MeOH. The electron density removed was accounted for in terms of added solvent molecules and these were added to the formulae and all appropriate numbers.

PXRD data were collected at 295 K in transmission mode using a *Stoe Stadi P* diffractometer equipped with CuKα1 radiation (Ge(111) monochromator and a *DECTRIS MYTHEN 1 K* detector). Whole-pattern profile matching analysis[35–37] of the diffraction patterns was done using the package FULLPROF SUITE (v. January 2021)[36,37] applying a previously determined instrument resolution function based on a NIST640d standard. The structural models were derived from the single crystal X-ray diffraction data. Refined parameters in *Rietveld* were scale factor, zero shift, lattice parameters, background points, sulfur atomic positions and peak shapes as a *Thompson–Cox–Hastings pseudo-Voigt* function. Preferred orientations as a *March–Dollase* multi-axial phenomenological model were incorporated into the analysis.

Ligand **1**·*CHCl*$_3$

$C_{49}H_{45}Cl_3N_6O_2$, $M_r = 856.26$, colorless block, monoclinic, space group $P2_1/c$, $a = 12.4528(3)$, $b = 17.0985(4)$, $c = 9.8901(3)$ Å, $\beta = 95.032(2)°$, $V = 2097.73(10)$ Å^3, $D_c = 1.356$ g cm^{-3}, $T = 150$ K, $Z = 2$, $\mu(CuK_\alpha) = 2.365$ mm^{-1}, 13047 reflections measured, 4072 unique ($R_{int} = 0.0459$). Refinement of 3495 reflections (278 parameters) with $I > 2\sigma(I)$ converged at final $R_1 = 0.1296$ (R_1 all data = 0.1440), $wR_2 = 0.2793$ (wR_2 all data = 0.2911), gof = 1.021. CCDC-2204762.

$[Co(NCS)_2(\mathbf{1})]_n \cdot 2nC_6H_4Cl_2$

$C_{62}H_{52}Cl_4CoN_8O_2S_2$, $M_r = 1205.96$, pink block, monoclinic, space group $P2_1/c$, $a = 14.5686(3)$, $b = 15.4967(2)$, $c = 16.2412(3)$ Å, $\beta = 115.8540(10)°$, $V = 3299.69(10)$ Å^3, $D_c = 1.214$ g cm^{-3}, $T = 150$ K, $Z = 2$, $\mu(CuK_\alpha) = 4.479$ mm^{-1}, 31299 reflections measured, 6498 unique ($R_{int} = 0.0493$). Refinement of 5392 reflections (329 parameters) with $I > 2\sigma(I)$ converged at final $R_1 = 0.1409$ (R_1 all data = 0.1579), $wR_2 = 0.3042$ (wR_2 all data = 0.3143), gof = 0.980. CCDC-2204764.

$[Co(NCS)_2(\mathbf{2})]_n \cdot 4nC_6H_4Cl_2$

$C_{76}H_{64}Cl_8CoN_8O_2S_2$, $M_r = 1528.00$, pink block, monoclinic, space group $P2_1/n$, $a = 16.1522(4)$, $b = 13.7867(3)$, $c = 17.1059(4)$ Å, $\beta = 111.381(2)°$, $V = 3547.07(15)$ Å^3, $D_c = 1.431$ g cm^{-3}, $T = 150$ K, $Z = 2$, $\mu(GaK_\alpha) = 3.814$ mm^{-1}, 62521 reflections measured, 6851 unique ($R_{int} = 0.0691$). Refinement of 5483 reflections (418 parameters) with $I > 2\sigma(I)$ converged at final $R_1 = 0.0594$ (R_1 all data = 0.0802), $wR_2 = 0.1472$ (wR_2 all data = 0.1683), gof = 1.072. CCDC-2204763.

$[Co_2(NCS)_4(\mathbf{2})_2]_n \cdot 5.5nCHCl_3 \cdot 0.2n$MeOH

$C_{109.90}H_{103.10}Cl_{16.50}Co_2N_{16}O_{4.40}S_4$, $M_r = 2549.40$, orange block, monoclinic, space group $C2/c$, $a = 37.8243(5)$, $b = 17.4894(2)$, $c = 27.6601(4)$ Å, $\beta = 135.1620(10)°$, $V = 12901.9(3)$ Å^3, $D_c = 1.312$ g cm^{-3}, $T = 150$ K, $Z = 4$, $\mu(CuK_\alpha) = 6.191$ mm^{-1}, 119069 reflections measured, 12759 unique ($R_{int} = 0.0640$). Refinement of 9771 reflections (695 parameters) with $I > 2\sigma(I)$ converged at final $R_1 = 0.1360$ (R_1 all data = 0.1553), $wR_2 = 0.3477$ (wR_2 all data = 0.3710), gof = 1.051. CCDC-2204766.

$[Co(NCS)_2(\mathbf{3})]_n \cdot 2.5nC_6H_5Cl$

$C_{69}H_{52.5}Cl_{2.5}CoN_8O_2S_2$, $M_r = 1237.36$, pink block, monoclinic, space group $P2_1/n$, $a = 15.0141(2)$, $b = 14.5575(3)$, $c = 16.8220(2)$ Å, $\beta = 115.0370(10)°$, $V = 3331.26(9)$ Å^3, $D_c = 1.234$ g cm^{-3}, $T = 130$ K, $Z = 2$, $\mu(GaK_\alpha) = 2.662$ mm^{-1}, 43829 reflections measured, 6694 unique ($R_{int} = 0.0607$). Refinement of 5387 reflections (369 parameters) with $I > 2\sigma(I)$ converged at final $R_1 = 0.0980$ (R_1 all data = 0.1139), $wR_2 = 0.2424$ (wR_2 all data = 0.2521), gof = 1.040. CCDC-2204765.

Supplementary Material

Supporting information for this article is available on the WWW under https://doi.org/10.1002/hlca.202200131. *Figures S1–S9*: NMR spectra of compounds **1a**, **2a**, **1b** and **2b**. *Figures S10* and *S11*: Mass spectra of compounds **1b** and **2b**. *Figures S12–S15*: Solid-state IR spectra of the compounds **1a**, **2a**, **1b** and **2b**. *Figures S16–S23*: NMR spectra of the ligands **1** and **2**. *Figures S24–S27*: Mass spectra of the ligands **1** and **2**. *Figures S28* and *S29*: Solid-state IR spectra of the ligands **1** and **2**. *Figures S30–S33*: Structural figures with atom numbering. *Figures S34–S37*: Solid-state IR

spectra of the coordination compounds $[Co(NCS)_2(\mathbf{1})]_n \cdot 2n C_6H_4Cl_2$, $[Co(NCS)_2(\mathbf{2})]_n \cdot 4n C_6H_4Cl_2$, $[Co_2(NCS)_4(\mathbf{2})_2]_n \cdot 5.5n CHCl_3 \cdot 0.2n MeOH$ and $[Co(NCS)_2(\mathbf{3})]_n \cdot 2.5n C_6H_5Cl$.

Acknowledgements

We acknowledge the support of the *Swiss National Science Foundation* (grant number 200020_182559) and the University of Basel.

Data Availability Statement

Data will be made available on zenodo.org.

Author Contribution Statement

Experimental: *S. S. C.* and *G. M.*; Crystallography: *G. M.* and *A. P.*; powder diffraction and analysis: *S. S. C.* and *G. M.*; manuscript writing and structure analysis: *S. S. C.*, *G. M.* and *C. E. H.*; manuscript editing: all authors; funding, project concepts and supervision: *C. E. H.* and *E. C. C.* All authors have read and agreed to the published version of the manuscript.

References

[1] C. E. Housecroft, 'Divergent 4,2′:6′,4″- and 3,2′:6′,3″-terpyridines as linkers in 2- and 3-dimensional architectures', *CrystEngComm* **2015**, *17*, 7461–7468.
[2] C. E. Housecroft, E. C. Constable, 'Ditopic and Tetratopic 4,2′:6′,4″-Terpyridines as Structural Motifs in 2D- and 3D-Coordination Assemblies', *Chimia* **2019**, *73*, 462–467.
[3] C. E. Housecroft, E. C. Constable, 'The terpyridine isomer game: from chelate to coordination network building block', *Chem. Commun.* **2020**, *56*, 10786–10794.
[4] C. E. Housecroft, E. C. Constable, 'Isomers of Terpyridine as Ligands in Coordination Polymers and Networks Containing Zinc(II) and Cadmium(II)', *Molecules* **2021**, *26*, 3110.
[5] R. R. Panicker, A. Sivaramakrishna, 'Remarkably flexible 2,2′:6′,2″-terpyridines and their group 8–10 transition metal complexes – Chemistry and applications', *Chem. Rev.* **2022**, *459*, 214426 and references therein.
[6] J. Grafino, M. Vargas, M. T. Garland, A. Ibáñez, R. Gaviño, R. Baggio, 'The novel ligand 4′-phenyl-3,2′:6′,3″-terpyridine (**L**) and the supramolecular structure of the dinuclear complex $[Zn_2(\mu\text{-L})(acac)_4] \cdot H_2O$ (acac = acetylacetonato)', *Inorg. Chem. Comm.* **2008**, *11*, 1388–1391.
[7] C. R. Groom, I. J. Bruno, M. P. Lightfoot, S. C. Ward, 'The Cambridge Structural Database', *Acta Crystallogr., Sect. B* **2016**, *72*, 171–179.
[8] I. J. Bruno, J. C. Cole, P. R. Edgington, M. Kessler, C. F. Macrae, P. McCabe, J. Pearson, R. Taylor, 'New software for searching the Cambridge Structural Database and visualising crystal structures', *Acta Crystallogr., Sect. B* **2002**, *58*, 389–397.
[9] J.-Y. Cheng, F.-W. Ding, P. Wang, C.-W. Zhao, Y.-B. Dong, 'Synthesis, Structure, and Ligand-Centered Catalytic Properties of M^{II} Coordination Polymers (M=Zn^{II}, Cd^{II}, Hg^{II}) with Open Pyridyl *N*-Oxide Sites', *ChemPlusChem* **2016**, *81*, 743–751.
[10] M. Zhao, J. Tan, J. Su, J. Zhang, S. Zhang, J. Wu, Y. Tian, 'Syntheses, crystal structures and third-order nonlinear optical properties of two series of Zn(II) complexes using the thiophene-based terpyridine ligands', *Dyes Pigm.* **2016**, *130*, 216–225.
[11] Y. M. Klein, A. Lanzilotto, A. Prescimone, K. W. Krämer, S. Decurtins, S.-X. Liu, E. C. Constable, C. E. Housecroft, 'Coordination behavior of 1-(3,2′:6′,3″-terpyridin-4′-yl)ferrocene: structure and magnetic and electrochemical properties of a tetracopper dimetallomacrocycle', *Polyhedron* **2017**, *129*, 71–76.
[12] J. Granifo, R. Gaviño, E. Freire, R. Baggio, 'The new sulphur-containing ligand 4′-(4-methylthiophenyl)-3,2′:6′,3″-terpyridine (**L1**) and the supramolecular structure of the dinuclear complex $[Zn_2(\mu\text{-}\mathbf{L1})(acac)_4]$ (acac = acetylacetonato): The key role of non-covalent S···O contacts and C–H···S hydrogen bonds', *J. Mol. Struct.* **2011**, *1006*, 684–691.
[13] D. Rocco, A. Prescimone, E. C. Constable, C. E. Housecroft, 'Switching the Conformation of 3,2′:6′,3″-tpy Domains in 4′-(4-*n*-Alkyloxyphenyl)-3,2′:6′,3″-Terpyridines', *Molecules* **2020**, *25*, 3162.
[14] Y. Watanabe, D. Yokoyama, T. Koganezawa, H. Katagiri, T. Ito, S. Ohisa, T. Chiba, H. Sasabe, J. Kido, 'Control of Molecular Orientation in Organic Semiconductor Films using Weak Hydrogen Bonds', *Adv. Mater.* **2019**, *31*, 1808300.
[15] X. Tian, Y. Zhu, M. Zhang, J. Tan, Q. Zhang, X. Wang, J. Yang, H. Zhou, J. Wu, Y. Tian, 'Mild acidic-enhanced mitochondrial-targeting by a neutral thiophene based terpyridine molecule with large two-photon action cross-section', *Dyes Pigm.* **2017**, *139*, 431–439.
[16] W. Du, H. Wang, Y. Zhu, X. Tian, M. Zhang, Q. Zhang, S. C. De Souza, A. Wang, H. Zhou, Z. Zhang, J. Wu, Y. Tian, 'Highly Hydrophilic, Two-photon Fluorescent Terpyridine Derivatives Containing Quaternary Ammonium for Specific Recognizing Ribosome RNA in Living Cells', *ACS Appl. Mater. Interfaces* **2017**, *9*, 31424–31432.
[17] Y. Shi, K. Wang, Y. Tsuchiya, W. Liu, T. Komino, X. Fan, D. Sun, G. Dai, J. Chen, M. Zhang, C. Zheng, S. Xiong, X. Ou, J. Yu, J. Jie, C.-S. Lee, C. Adachi, X. Zhang, 'Hydrogen bond-modulated molecular packing and its applications in high-performance non-doped organic electroluminescence', *Mater. Horiz.* **2020**, *7*, 2734–2740.
[18] Y.-Z. Shi, K. Wang, S.-L. Zhang, X.-C. Fan, Y. Tsuchiya, Y.-T. Lee, G.-L. Dai, J.-X. Chen, C.-J. Zheng, S.-Y. Xiong, X.-M. Ou, J. Yu, J.-S. Jie, C.-S. Lee, C. Adachi, X.-H. Zhang, 'Characterizing the Conformational Distribution in an Amorphous Film of an Organic Emitter and Its Application in a "Self-Doping" Organic Light-Emitting Diode', *Angew. Chem. Int. Ed.* **2021**, *60*, 25878–25883.

[19] C. Zhang, Y. Zhao, D. Li, J. Liu, H. Han, D. He, X. Tian, S. Li, J. Wu, Y. Tian, 'Aggregation-induced emission (AIE)-active molecules bearing singlet oxygen generation activities: the tunable singlet–triplet energy gap matters', *Chem. Commun.* **2019**, *55*, 1450–1453.
[20] X. Guo, M. Bian, F. Lv, Y. Wang, Z. Zhao, Z. Bian, B. Qu, L. Xiao, Z. Chen, 'Increasing electron transporting properties and horizontal molecular orientation *via meta*-position of nitrogen for "$(A)_n$–D–$(A)_n$" structured terpyridine electron-transporting material', *J. Mater. Chem. C* **2019**, *7*, 11581–11587.
[21] J. Zhang, H. Wang, 'Photophysical investigaions and the bioimaings of α-, β-, γ-pyridine-based terpyridine derivatives', *J. Mol. Struct.* **2018**, *1157*, 457–462.
[22] Y. M. Klein, A. Prescimone, E. C. Constable, C. E. Housecroft, 'Coordination behaviour of 1-(4,2′:6′,4″-terpyridin-4′-yl)ferrocene and 1-(3,2′:6′,3″-terpyridin-4′-yl)ferrocene: predictable and unpredictable assembly algorithms', *Aust. J. Chem.* **2017**, *70*, 468–477.
[23] Y. M. Klein, E. C. Constable, C. E. Housecroft, A. Prescimone, 'A 3-dimensional $\{4^2.8^4\}$ lvt net built from a ditopic bis(3,2′:6′,3″-terpyridine) tecton bearing long alkyl tails', *CrystEngComm* **2015**, *17*, 2070–2073; correction: *CrystEngComm* **2022**, *24*, 5170–5170.
[24] G. Manfroni, A. Prescimone, S. R. Batten, Y. M. Klein, D. J. Gawryluk, E. C. Constable, C. E. Housecroft, 'Trinodal Self-Penetrating Nets from Reactions of 1,4-Bis(alkoxy)-2,5-bis(3,2′:6′,3″-terpyridin-4′-yl)benzene Ligands with Cobalt(II) Thiocyanate', *Crystals* **2019**, *9*, 529.
[25] S. S. Capomolla, G. Manfroni, A. Prescimone, E. C. Constable, C. E. Housecroft, 'A Tail Does Not Always Make a Difference: Assembly of *cds* Nets from Co(NCS)2 and 1,4-bis(*n*-Alkyloxy)-2,5-bis(3,2′:6′,3″-terpyridin-4′-yl)benzene Ligands', *Molecules* **2022**, *27*, 4995.
[26] G. Manfroni, B. Spingler, A. Prescimone, E. C. Constable, C. E. Housecroft, 'Multitopic 3,2′:6′,3″-terpyridine ligands as 4-connecting nodes in two-dimensional 4,4-networks', *CrystEngComm* **2022**, *24*, 7073–7082.
[27] J. Wang, G. S. Hanan, 'A Facile Route to Sterically Hindered and Non-Hindered 4′-Aryl-2,2′:6′,2″-Terpyridines', *Synlett* **2005**, 1251–1254.
[28] S. S. Capomolla, G. Manfroni, A. Prescimone, E. C. Constable, C. E. Housecroft, 'Versatility within (4,4) networks assembled from 1,4-bis(*n*-alkyloxy)-2,5-bis(3,2′:6′,3″-terpyridin-4′-yl)benzene and $[Cu(hfacac)_2]$ (Hhfacac = 1,1,1,5,5,5-hexafluoropentane-2,4-dione)', *Polyhedron* **2022**, *224*, 116005.
[29] C. Janiak, 'A critical account on π–π stacking in metal complexes with aromatic nitrogen-containing ligands', *Dalton Trans.* **2000**, 3885–3896.
[30] C. F. Macrae, I. Sovago, S. J. Cottrell, P. T. A. Galek, P. McCabe, E. Pidcock, M. Platings, G. P. Shields, J. S. Stevens, M. Towler, P. A. Wood, 'Mercury 4.0: from visualization to analysis, design and prediction', *J. Appl. Cryst.* **2020**, *53*, 226–235.
[31] L. Palatinus, G. Chapuis, 'SUPERFLIP - a computer program for the solution of crystal structures by charge flipping in arbitrary dimensions', *J. Appl. Cryst.* **2007**, *40*, 786–790.
[32] L. Palatinus, S. J. Prathapa, S. van Smaalen, '*EDMA*: a computer program for topological analysis of discrete electron densities', *J. Appl. Cryst.* **2012**, *45*, 575–580.
[33] O. V. Dolomanov, L. J. Bourhis, R. J. Gildea, J. A. K. Howard, H. Puschmann, '*OLEX2*: a complete structure solution, refinement and analysis program', *J. Appl. Cryst.* **2019**, *42*, 339–341.
[34] G. M. Sheldrick, 'Crystal structure refinement with *SHELXL*', *Acta Crystallogr., Sect. C* **2015**, *27*, 3–8.
[35] A. Le Bail, H. Duroy, J. L. Fourquet, 'Ab-initio structure determination of $LiSbWO_6$ by X-ray powder diffraction', *Mat. Res. Bull.* **1988**, *23*, 447–452.
[36] G. S. Pawley, 'Unit-cell refinement from powder diffraction scans', *J. Appl. Cryst.* **1981**, *14*, 357–361.
[37] J. Rodríguez-Carvajal, 'Recent advances in magnetic structure determination by neutron powder diffraction', *Physica B* **1993**, *192*, 55–69.
[38] T. Roisnel, J. Rodríguez-Carvajal, 'WinPLOTR: a Windows Tool for Powder Diffraction Patterns Analysis', in 'Materials Science Forum', Vol. 378–381, *Trans Tech Publications, Ltd.* **2001**, pp. 118–123.

Received October 10, 2022
Accepted November 4, 2022

